RSC Advances

PAPER

View Article Online
View Journal | View Issue

Cite this: *RSC Adv.*, 2025, **15**, 49679

Minor groove binding of imidocarb dipropionate to calf thymus DNA: insights from multispectral, thermodynamic, and molecular docking approaches

Yuxin Yu,†[a] Wanxin Luo,†[a] YiWen Zhong,[a] Dongfang Li,[a] Sen Wang,[a] Yidan Bai,[a] Junlong Zhao[a] and Lan He*[ab]

Received 5th October 2025
Accepted 4th November 2025

DOI: 10.1039/d5ra07575k

rsc.li/rsc-advances

This study aimed to investigate the interaction between imidocarb dipropionate (IMDP) and double-stranded DNA, as understanding its mechanism of action is crucial for optimizing its use as a veterinary antiprotozoal agent. Using calf thymus DNA as a model, we systematically explored the binding of IMDP to DNA *via* UV-vis absorption spectroscopy, Competitive displacement assays, thermal denaturation analysis, circular dichroism spectroscopy, ion interference experiments, viscosity measurement, and molecular docking. Results indicated that IMDP binds to DNA with a decrease in hypochromicity rates of 23.95% and 22.17%. Notably, the T_m value rose from 69 °C to 71 °C upon binding, and the circular dichroism spectrum peaks remained nearly unchanged, suggesting a groove binding mode with minimal impact on DNA conformation and viscosity. Our findings confirm that IMDP binds to double-stranded DNA by interacting within the DNA groove, supporting its potential as a DNA-targeting antiparasitic drug.

1 Introduction

DNA, as the carrier of genetic information, plays a pivotal role in life processes by directing protein synthesis and cellular functions. Since the discovery of its double-helix structure, DNA has emerged as a prime therapeutic target for diverse small molecules ranging from anticancer agents to antibiotics.[1,2] The growing interest in DNA–drug interactions stems from their importance in understanding pharmacological mechanisms and designing novel therapeutics.[3,4] These interactions primarily manifest through covalent bonding or noncovalent modalities such as electrostatic forces, groove binding, and intercalation.[5–7] Despite the availability of genomic data and structural insights, DNA-based drug targets remain underexplored compared with protein targets, underscoring the need for systematic studies on molecular binding mechanisms and influencing factors.[8]

The therapeutic potential of DNA targeting is particularly evident in parasitic disease management. Recent advances highlight DNA as a strategic intervention point against protozoan infections.[9,10] For example, pyrimethamine exerts antimalarial effects by disrupting parasite DNA synthesis through dihydrofolate reductase inhibition,[11,12] whereas metronidazole induces protozoan DNA damage in giardiasis treatment.[13] Such successes have spurred investigations into parasite-specific DNA vulnerabilities to combat drug resistance and improve therapeutic precision.[14–16] However, the molecular intricacies of many antiparasitic agents remain poorly characterized.

Imidocarb dipropionate (IMDP), a synthetic aromatic diamidine with dual amide functionalities,[17] exemplifies this knowledge gap. It can treat various parasitic diseases, including those caused by *Trypanosomes* and *Babesia*,[18–20] yet its molecular interactions with parasitic or host DNA remain unclear. This lack of mechanistic understanding hinders rational optimization of its antiprotozoal activity and safety profile.

In this study, we systematically investigated the binding behavior of IMDP with calf thymus DNA (Ct-DNA) using techniques such as UV-vis spectroscopy, fluorescence quenching, circular dichroism, DNA melting analysis, viscosity measurements, and molecular docking, elucidating the interaction patterns between the two.

2 Experimental

2.1. Materials

IMDP was purchased from J&K Scientific, China. Ct-DNA, acridine orange (AO), and Hoechst 33258 were procured from

[a]*National Key Laboratory of Agricultural Microbiology, College of Veterinary Medicine, Huazhong Agricultural University, Wuhan, Hubei 430070, China. E-mail: yuyuxin@webmail.hzau.edu.cn; luowanxin@webmail.hzau.edu.cn; zhongyiwen@webmail.hzau.edu.cn; dongfang0216@webmail.hzau.edu.cn; senwang@webmail.hzau.edu.cn; byd123@webmail.hzau.edu.cn; zhaojunlong@mail.hzau.edu.cn; helan@mail.hzau.edu.cn*

[b]*Hubei Jiangxia Laboratory, Wuhan 430200, China*

† These authors contributed equally.

Sigma Aldrich, USA. Tris–HCl and sodium chloride (NaCl) were obtained from Thermo Fisher Scientific, USA. The Wuhan strain of *Babesia gibsoni* (designated *B. gibsoni* WH), which has been maintained through continuous *in vitro* culture, is preserved in the Laboratory of Parasitology at Huazhong Agricultural University. All other solvents and chemicals were of reagent grade.

2.2. Instrumentations

The absorption spectra were measured on a dual beam UV-vis spectrophotometer UV-2600 (Shimadzu, Japan) fitted with a thermostat bath using 1 × 1 cm quartz cuvettes. Fluorescence measurements were performed on a Shimadzu RF-5301PC spectrophotometer (Japan) coupled with a Peltier and equipped with a xenon flash lamp using 1.0 cm quartz cells. The excitation and emission slit widths were set at 5.0 nm. The CD spectra were recorded on a J-1500 CD spectrophotometer (JASCO, Japan) using a quartz cuvette with a path length of 1.0 mm. The measurement of DNA viscosity was performed *via* an Ubbelohde viscometer.

2.3. Sample preparation

The stock solution of IMDP (10 mM) was dissolved in ultrapure water, followed by dilution with 10 mM Tris–HCl buffer solution (pH 7.2) for later use. The Ct-DNA was dissolved in 10 mM Tris–HCl buffer solution and stored at −20 °C. The purity of the DNA was confirmed by measuring the A_{260}/A_{280} ratio, indicating that no further purification was necessary. The concentration of the DNA mixture was determined *via* the average molar extinction coefficient of a single nucleotide at a wavelength of 260 nm, which is 6600 M^{-1} cm^{-1}.[21]

2.4. UV absorbance spectra

UV spectra of the IMDP and IMDP-Ct-DNA complexes were recorded at 25 °C in the wavelength range of 210–340 nm. The concentration of Ct-DNA was fixed at 60 μM, and then different concentrations of Ct-DNA (0–70 μM) were titrated. Then, 10 mM Tris–HCl buffer (pH 7.2) was added to bring the volume of the reaction mixture to 3 mL. Baseline correction was performed using 10 mM Tris–HCl buffer as a blank solution to observe UV spectra unique to the IMDP-Ct-DNA complex only, and each experiment was repeated three times.[22]

2.5. Competitive displacement assays

Ct-DNA (50 μM) and acridine orange (AO, 5 μM) were codissolved in 3.0 mL of Tris–HCl buffer (10 mM, pH 7.4). The mixture was vortexed thoroughly and transferred into a 1.0 cm quartz cuvette. A gradient titration method was used to sequentially add IMDP stock solution (50 mM), increasing the final IMDP concentration from 0 to 90 μM (in 10 μM increments). At each concentration step, the system was equilibrated at room temperature for 5 min to ensure binding equilibrium. Emission spectra (300–700 nm) were recorded at an excitation wavelength of 502 nm, with triplicate scans averaged for each sample.[23]

Similarly, a complex of Ct-DNA (50 μM) and Hoechst 33258 (5 μM) was prepared in an identical buffer system. For this system, the excitation wavelength was set to 352 nm, and the IMDP titration range was adjusted to 0–30 μM (10 μM increments). All other experimental conditions, including equilibration time, spectral acquisition parameters, and data averaging protocols, remained consistent with the aforementioned procedure.

2.6. DNA melting assay

Ct-DNA and IMDP were separately dissolved in 10 mM Tris–HCl buffer (pH 7.4) to prepare two systems: (1) the experimental group, which contained equimolar concentrations (60 μM) of the Ct-DNA/IMDP complex, and (2) the control group, which contained only 60 μM Ct-DNA. Both systems were adjusted to a total volume of 3.0 mL. Following vortex mixing, the samples were transferred into a 1.0 cm pathlength high-precision quartz cuvette. The temperature was linearly increased from 20 °C to 100 °C *via* a thermostatically controlled metal bath. At 5 °C intervals, the absorbance at 260 nm (A_{260}) was measured *via* a UV-2600 spectrophotometer (Shimadzu Corporation, Japan), and the data were recorded for subsequent thermal denaturation analysis.

2.7. Circular dichroism studies

A 10 μM IMDP solution was mixed with a 100 μM Ct-DNA solution at a 1 : 1 volume ratio within a 10 mM Tris–HCl buffer system (pH 7.4) at room temperature. The mixture was then incubated in the dark at room temperature for 30 min to ensure complete intermolecular binding. Circular dichroism (CD) spectra were acquired *via* a J-1500 spectropolarimeter (JASCO, Japan) equipped with a 0.2 cm pathlength high-precision quartz cuvette. Spectral measurements were performed across the characteristic absorption range of 220–320 nm, with a step size of 1 nm, bandwidth of 1 nm, and scanning speed of 100 nm min^{-1}. Three consecutive scans were averaged to enhance signal reproducibility. Prior to the measurements, baseline correction was performed using the same batch of buffer solution. All the raw spectra underwent Savitzky–Golay smoothing (5-point window width, second-order polynomial fitting) to minimize noise artifacts. To eliminate solvent background interference, the final spectra were obtained by subtracting the blank buffer signal and normalizing to the molar ellipticity ($\Delta\varepsilon$, M^{-1} cm^{-1}) for quantitative analysis.

2.8. Ion interference experiment

A 20 μM IMDP solution and a 60 μM Ct-DNA solution were mixed in 3 mL of 10 mM Tris–HCl buffer (pH 7.4) and incubated at room temperature for 15 min. A separate control system containing 60 μM Ct-DNA alone was prepared in the same buffer. To both the Ct-DNA solution and the preformed IMDP-CtDNA complex system, stepwise additions of NaCl solution (in a concentration gradient ranging from 1 mM to 10 mM) were performed. After each addition, the mixtures were vortexed thoroughly and allowed to equilibrate at room temperature for 3 min to ensure a complete reaction. The absorbance values of all the reaction solutions at 260 nm (A_{260}) were subsequently

measured *via* a UV-vis spectrophotometer (model and manufacturer details, if required).

2.9. Viscosity measurement

Viscosity measurements were performed while keeping the DNA concentration constant (50 M) and varying the concentration of IMDP. Viscosity measurements were carried out with a Ubbelohde viscometer suspended vertically in a thermostat at 25 °C. A digital stopwatch was used to measure the flow time. To obtain an average calculation time, each sample was tested three times. The data are presented as $(\eta/\eta_0)^{1/3}$ *versus* the ratio of the IMDP/DNA concentration. Here, η and η_0 are the viscosities of DNA in the presence and absence of the IMDP, respectively.

2.10. Molecular docking

The molecular docking experiment was performed *via* AutoDock 4.2.6 software. The crystal structure of IMDP was obtained from the SciFinder database, and polar hydrogen atoms and Gasteiger charges were incorporated *via* AutoDock tools. The ligand binding site of IMDP was identified, and its rotatable bonds were determined.

The structure of the B-DNA dodecamer 5′-d (CGCGAATTCGCG)$_2$-3′ (PDBID:1BNA) was retrieved from the Protein Data Bank (PDB).[24] To facilitate docking calculations with the AutoDock tool, this structure underwent further modifications, including removal of all water molecules, addition of Gasteiger charges, and necessary hydrogen atoms.

The Lamarckian genetic algorithm in AutoDock was employed to simulate interactions between the IMDP and DNA. A grid box with a spacing of 0.392 Å containing 64 × 72 × 126 grid points was prepared to cover the entire DNA-binding site while allowing for ligand mobility.

All other parameters were set according to default values provided by AutoDock. The grid energy in the docking pocket region was computed *via* AutoGrid software. A total of 100 genetic algorithm runs were performed to identify the best structure on the basis of the lowest binding free energy.

3 Results and discussion

3.1. UV-vis spectroscopy

As illustrated in Fig. 1, in the absence of Ct-DNA (0 nM), the absorption spectrum of IMDP exhibited two characteristic peaks: a primary peak at 208 nm and a secondary peak at 256 nm. The emergence of the primary peak (208 nm) is attributed to the n → π* electronic transition within the imidazole ring of IMDP, which contains lone electron pairs localized on nitrogen atoms.[25] Such transitions typically occur in the 200–230 nm range. The secondary peak (256 nm) originates from the π → π* transition of the conjugated system formed by the benzene ring and the nitroimine group (–N–NO_2) in IMDP. This transition aligns with the expected spectral range of 250–280 nm for aromatic π → π* transitions, which is consistent with experimental observations.[26]

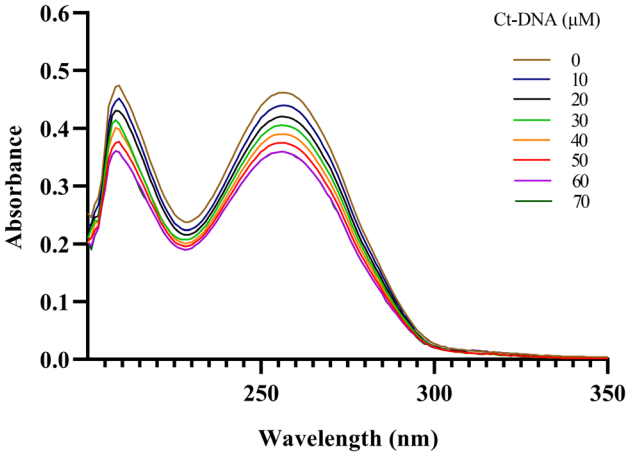

Fig. 1 UV-vis absorption spectra of IMDP (60 μM) solutions in the absence and presence of various concentrations of Ct-DNA (0 to 70 μM) at 298 K and pH = 7.4.

With the gradual increase in Ct-DNA concentration (0 to 60 nM), a progressive reduction in absorption intensity was observed for both the primary and secondary peaks, indicative of a hypochromic shift. This phenomenon suggests the formation of a ground-state complex between IMDP and Ct-DNA, likely mediated by intercalative or groove-binding interactions that perturb the electronic transitions of IMDP, and the absorption maxima exhibited no significant shift. The observed percentage hypochromicity (% *H*) was 23.95% and 22.17%, which was calculated *via* the following equation:

$$\% H = (A_0 - A_F)/A_0 \times 100$$

where A_0 is the absorption of the IMDP in the absence of Ct-DNA and where A_F is the final value of absorption when there was no change due to the further successive addition of Ct-DNA to the IMDP solution.

Upon comprehensive literature analysis, it has become evident that intercalative agents characteristically elicit a pronounced hypochromic effect (hypochromism ≥25%) in the ultraviolet absorption spectrum upon binding to double-stranded DNA. In contrast, groove-binding drugs typically induce a markedly lower hypochromism (<25%) or even negligible changes.[27–29] As in the present spectra, no redshift was observed, and the hypochromic shift was <25%; thus, we can rule out intercalative binding. The above results suggest that there can be a groove or electrostatic binding present in the IMDP-Ct-DNA system.[30–33]

3.2. Competitive displacement assays

Competitive displacement assays involve the addition of IMDP to a complex system containing Ct-DNA-fluorescent ligands. If IMDP can bind to Ct-DNA, it will cause changes in the emission spectrum of the complex. The decrease in fluorescence resulting from the introduction of a second ligand is commonly interpreted as displacement of the fluorescent probe by the ligand.[34]

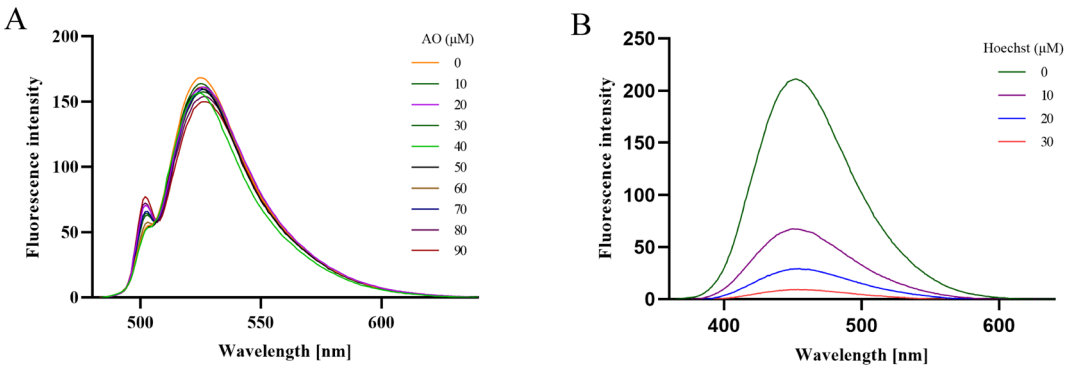

Fig. 2 Competitive displacement assays demonstrating the binding specificity of IMDP-DNA. (A) Fluorescence spectra of the Ct-DNA (50 μm) and AO (5 μM) complexes in the presence of varying concentrations of IMDP (0–90 μM). (B) Fluorescence spectra of Ct-DNA (50 μM) and the Hoechst 33258 (5 μM) complex in the presence of varying concentrations of IMDP (0–30 μM).

Hoechst 33258 and acridine orange are fluorescent dyes that can bind to double-stranded DNA, generating fluorescence with diverse applications in biological research.[35] Acridine orange (AO) primarily binds to DNA through insertion, wherein the acridine orange molecule becomes embedded between the base pairs of the DNA double helix, forming a sandwich-like structure.[36] This insertion disrupts the normal DNA structure, leading to changes in the fluorescent properties of acridine orange on the basis of its binding state with DNA. Fig. 2A shows the fluorescence emission spectrum of AO-Ct-DNA. Following the addition of IMDP, there was no significant change in the fluorescence intensity of the AO-DNA system. This finding indicates that IMDP does not displace AO in DNA and may bind to DNA through a noninsertional mode.

To further investigate the binding mode of IMDP to DNA, we hypothesized that IMDP and DNA were bound *via* groove binding and conducted Hoechst substitution experiments. Hoechst 33258 is capable of permeating cell membranes and binding to the minor groove of DNA double strands, particularly in regions abundant in adenine and thymine (A/T). The fluorescence of Hoechst was weak in aqueous solution, but the fluorescence intensity of the Hoechst-Ct-DNA system was significantly enhanced after binding with DNA. As shown in Fig. 2B, upon the addition of IMDP, the fluorescence intensity of Hoechst-Ct-DNA decreased significantly with increasing IMDP concentration, confirming once again that IMDP does not bind to DNA through the insertion mode but interacts with DNA *via* groove binding.

3.3. DNA melting assay

Thermal denaturation experiments serve as a robust method for investigating the binding modes of small molecules with DNA. The double-helical structure of DNA is stabilized by hydrogen bonding and base-stacking interactions. Upon heating, these stabilizing forces weaken, leading to strand separation into single-stranded DNA. The melting temperature (T_m) corresponds to the temperature at which 50% of the duplex DNA dissociates into single strands. Ligand–DNA interactions can significantly modulate T_m: extensive studies have demonstrated that intercalative binding typically induces a significantly larger elevation in DNA melting temperature ($\Delta T_m \geq 5$–8 °C) than groove binding, with some intercalators producing ΔT_m values exceeding 10 °C. In contrast, groove-binding agents generally exert only a modest effect on T_m. Consequently, a ΔT_m of ≥5–8 °C is widely accepted as indicative of intercalation, whereas a $\Delta T_m < 5$ °C or no observable change is considered characteristic of groove binding,[37–39] whereas groove-binding or electrostatic interactions induce minimal or negligible shifts.[40–42]

As demonstrated in Fig. 3, the T_m of free Ct-DNA was 69.0 ± 1 °C. Upon addition of IMDP, the T_m increased marginally to 71 ± 1 °C. Although slight thermal stabilization was observed, the magnitude of this shift ($\Delta T_m \approx 2$ °C) falls far below the range expected for classical intercalators. This minor enhancement may arise from conformational adjustments in DNA base pairs induced by the binding of the IMDP minor groove, which

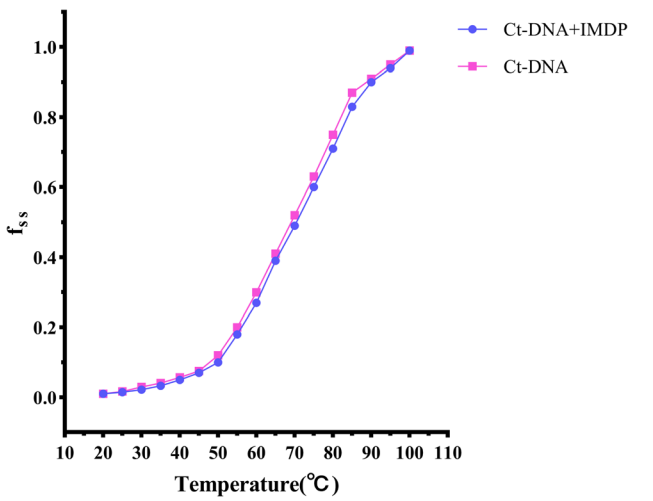

Fig. 3 Melting curves of Ct-DNA (60 M) in the absence and presence of IMDP (60 M), where FSS represents the ratio of the absorbance of Ct-DNA with increasing temperature (20–100 °C) and the absorbance at 20 °C. Only a slight increase in the melting temperature of Ct-DNA was observed in the presence of IMDP, suggesting nonintercalative binding between IMDP and DNA.

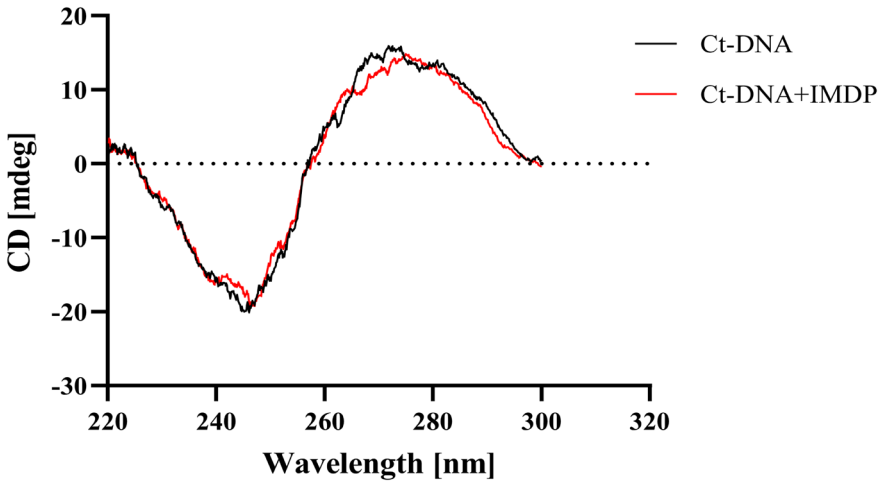

Fig. 4 Circular dichroism (CD) spectra of calf thymus DNA (Ct-DNA, 100 μM) in 10 mm Tris–HCL buffer (pH 7.2) before (black line) and after (red line) the addition of IMDP.

indirectly stabilizes the duplex structure. These results further corroborate that IMDP interacts with Ct-DNA *via* a groove-binding mode, which is consistent with findings from competitive displacement assays.

3.4. Circular dichroism studies

The interaction of small molecules with DNA can stabilize or destabilize the double-helical structure, thereby modulating its secondary conformation.[43,44] Such structural perturbations can be investigated *via* circular dichroism (CD) spectroscopy, a sensitive analytical technique capable of detecting conformational changes in the DNA phosphate backbone induced by ligand binding.[45] Canonical B-form DNA exhibits characteristic CD spectral features: a negative band at 245 nm (attributed to right-handed helicity) and a positive band at 275 nm (arising from base-stacking interactions). The intensity and positional shifts ($\Delta\lambda$) of these bands are highly sensitive to ligand-binding modes (*e.g.*, intercalation, groove binding, or electrostatic interactions), serving as critical spectroscopic indicators for elucidating DNA–ligand interaction mechanisms.

As shown in Fig. 4, groove-binding or electrostatically driven interactions induce minimal or negligible perturbations to the base-stacking band (275 nm) and helicity band (245 nm), whereas intercalative binding significantly reduces the intensity of both bands. Upon incremental addition of IMDP to Ct-DNA, the CD spectrum of B-form DNA exhibited no significant positional shifts in either the positive or negative bands. This observation indicates that IMDP interacts with Ct-DNA *via* a groove-binding mode. The subtle intensity changes observed post-IMDP addition may stem from a conformational transition of the nucleic acid structure from the canonical B-form to a more compact φ-form, which retains groove-bound ligand accommodation while altering base-pair tilt angles.

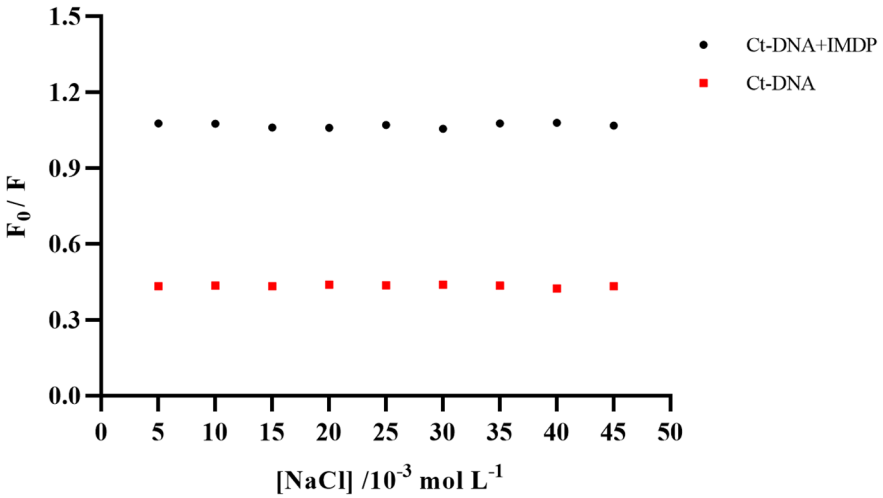

Fig. 5 Effect of ionic strength on the fluorescence intensity of the IMDP-DNA complex. F_0 represents the fluorescence intensity of the IMDP-DNA complex without NaCl, and F represents the fluorescence intensity of the AFB1–AFG1–DNA complex with NaCl.

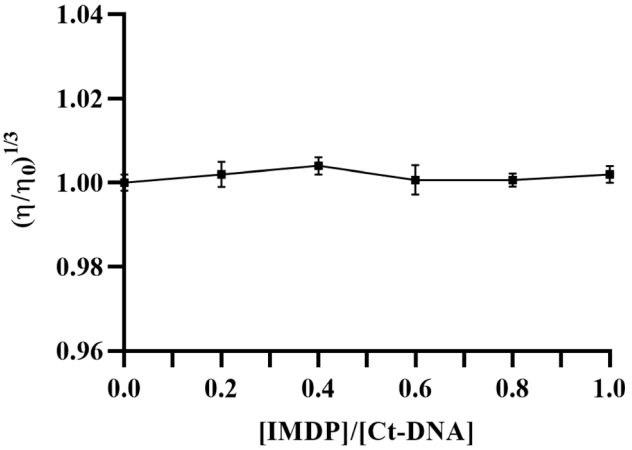

Fig. 6 Viscosity analysis of the IMDP-Ct-DNA interaction. The concentration of DNA was kept constant while the concentration of IMDP was varied. The data represent the means ± SDS of three experiments.

3.5. Ion interference experiment

To further elucidate the binding mode of IMDP with DNA, the ionic strength effect was utilized as a coefficient method.[46] The DNA double strand is an anionic polyelectrolyte with phosphate groups. In this investigation, the ionic strength of the system was modulated by NaCl. Upon dissolving NaCl, Na^+ ions are liberated, neutralizing the negative charges on the phosphate backbone of the DNA, thereby attenuating electrostatic repulsion and gradually increasing the degree of DNA chain compaction.[47] These ions compete with small molecules for binding sites on the phosphate backbone of DNA, resulting in an increase in the free concentration of small molecules in solution. When electrostatic interactions are involved in the binding mode, the addition of NaCl diminishes the degree of competition between NaCl and small molecules for DNA binding, as evidenced by the degree of fluorescence quenching.

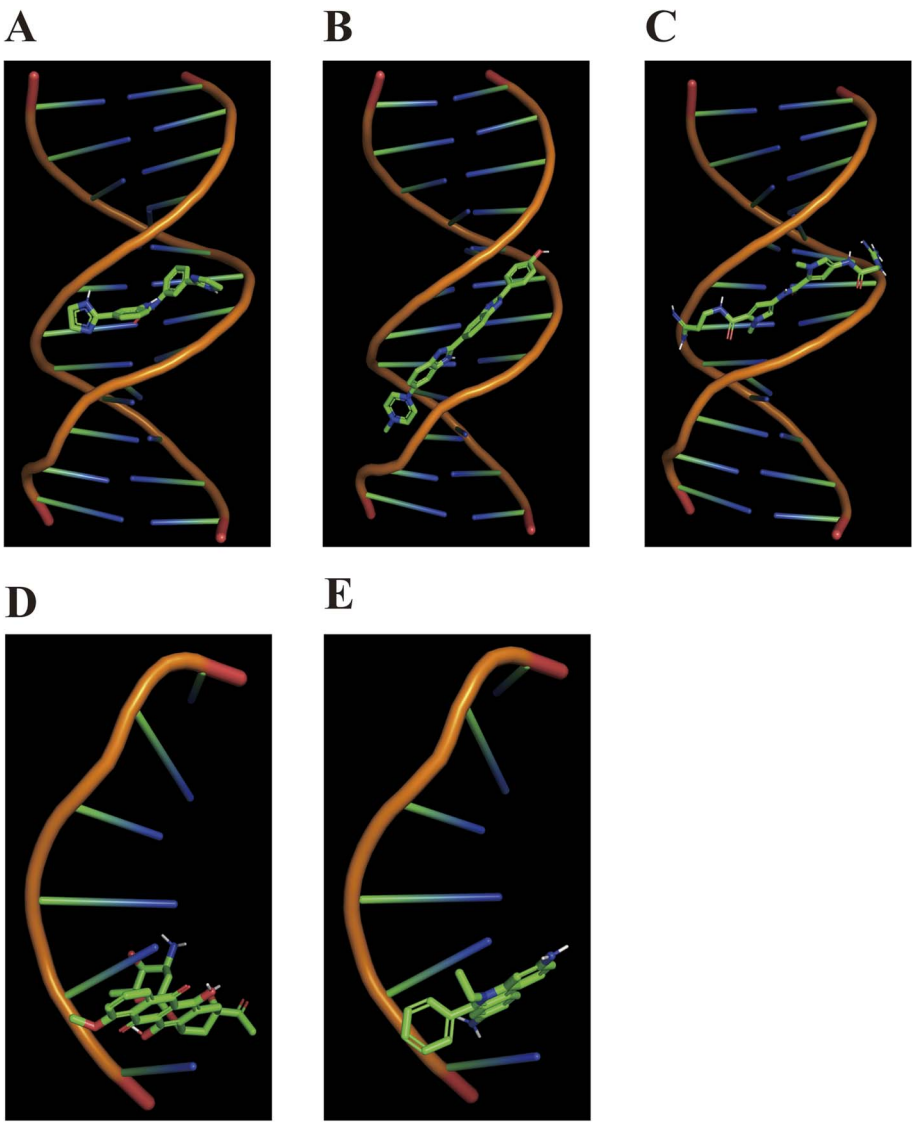

Fig. 7 The results of the molecular docking. (A–E) The results of the docking of IMDP, Hoechst, Netropsin, Daunorubicin, and Ethidium with DNA from (A) to (E).

To ascertain whether IMDP binds to DNA through electrostatic interactions, we investigated the effect of NaCl on the fluorescence intensity of the IMDP-DNA complex. In Fig. 5, F_0 represents the fluorescence intensity of the IMDP-DNA complex in the absence of NaCl, and F represents the fluorescence intensity in the presence of NaCl. As depicted in Fig. 5, no significant change in fluorescence intensity was observed after the addition of NaCl to the IMDP-DNA system. These results indicate that IMDP binds to Ct-DNA through a nonelectrostatic interaction mode, likely dominated by groove-binding or intercalative mechanisms.

3.6. Viscosity measurements

To further elucidate the binding mechanism of IMDP with Ct-DNA, viscosity measurements were performed.[48] Fluid dynamic techniques such as viscosity measurement are highly sensitive and can provide compelling evidence regarding the interaction of small molecules with DNA. In cases of insertion-type binding between small molecules and DNA, an increase in the separation of base pairs at the insertion site leads to an overall elongation of DNA, resulting in a significant increase in viscosity. However, when molecules interact with DNA through electrostatic or groove binding, there is minimal change in the viscosity of the DNA solution. As depicted in Fig. 6, no substantial increase in DNA viscosity is observed as the concentration of IMDP increases, providing robust evidence that IMDP interacts with DNA through groove binding rather than insertion-type binding. The initial slight decrease in DNA viscosity may be attributed to the curvature or twisting of the DNA helix caused by IMDP, which reduces its overall length and consequently lowers its viscosity.

3.7. Molecular docking

Molecular docking, a pivotal computational tool in rational drug discovery, was employed to investigate the interaction between the DNA (NDB ID: GDL001, NDB ID: DDF001) and compound.[49,50] The B-form DNA structure was retrieved from the Nucleic Acid Knowledgebase (NAKB), followed by the removal of crystallographic water molecules and cocrystallized ligands to generate a clean receptor model. The three-

Table 1 The docking score of IMDP, Hoechst, Netropsin, Daunorubicin and Ethidium

Compound ID	Structure	CDOCKER energy (kcal mol^{-1})
IMDP	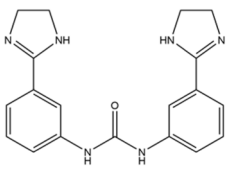	−10.87
Hoechst	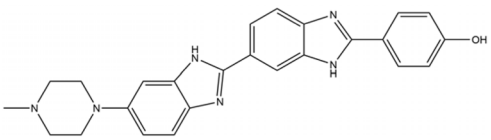	−12.1
Netropsin	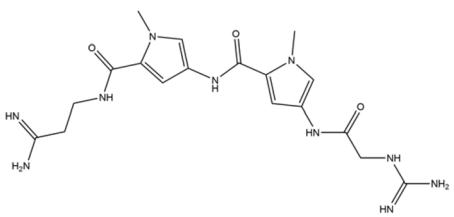	−9.19
Daunorubicin	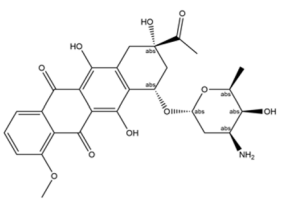	−4.81
Ethidium	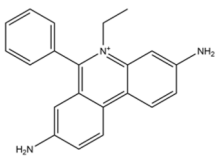	−4.96

dimensional structure of the compounds was geometrically optimized at the DFT/B3LYP/6-31G** level to ensure conformational accuracy. Molecular docking simulations were performed *via* AutoDock 4.2.6 with Lamarckian genetic algorithm parameters (150 populations, 2.5×10^6 energy evaluations, 100 independent runs). Cluster analysis of binding poses (RMSD tolerance: 2.0 Å) identified the lowest free energy conformation as the predominant binding mode.[51]

The results demonstrated that IMDP adopts a distinct spatial orientation when bound to B-DNA, exhibiting minor-groove binding characteristics through structural complementarity with the helical topology. As illustrated in Fig. 7, IMDP is preferentially located in the small grooves rich in at within the twelve-axis body, similar to the binding mode of classical groove-binding compounds such as hoechst and netropsin. As shown in Table 1, the binding energy of IMDP with DNA is similar to that of groove-binding compounds such as hoechst and netropsin and significantly lower than that of intercalating compounds like daunorubicin and ethidium. This result further confirms that IMDP interacts with DNA *via* a groove-binding mechanism.

Notably, the planar aromatic system of IMDP aligns parallel to the groove walls, avoiding base-pair intercalation—a finding that is consistent with experimental CD spectroscopy and thermal denaturation data. Comparative analysis with classical groove binders (*e.g.*, netropsin) revealed analogous spatial occupancy patterns but distinct hydrogen-bonding networks, suggesting the unique pharmacophoric features of IMDP. This computational evidence strongly supports a minor-groove-dominated binding mechanism, where both electrostatic complementarity and shape-selective hydrophobic interactions govern ligand–DNA recognition.

4 Conclusion

Since the late 20th century, imidocarb, diminazene, and atovaquone have served as first-line chemotherapeutic agents for treating babesiosis.[52,53] Despite the broad-spectrum antiprotozoal activity and extensive veterinary applications of imidocarb, significant research gaps persist compared with those associated with structurally related agents such as diminazene and atovaquone. Critical mechanistic questions remain unresolved, as its molecular targets and precise mechanism of action (MoA) remain incompletely characterized. This knowledge gap urgently requires systematic investigation to elucidate its pharmacodynamic profile and optimize its therapeutic utility.

This study provides the first systematic elucidation of the groove-binding specificity of imidocarb dipropionate (IMDP) with double-stranded DNA. The binding mode of IMDP with calf thymus DNA has been thoroughly characterized. Through integrated spectroscopic and computational analyses. UV-vis absorption spectroscopy revealed a concentration-dependent hypochromic effect ($\Delta A \approx 25\%$) without a λ_max shift, indicative of nonintercalative binding, a finding corroborated by fluorescence displacement assays. Specifically, IMDP failed to perturb the emission of intercalator-bound acridine orange (AO) but significantly quenched Hoechst 33258-DNA fluorescence ($\Delta F = 63\%$), demonstrating the selective displacement of the minor groove probe.

Thermal denaturation experiments provided complementary evidence: the modest T_m increase ($\Delta T_m \approx 2$ °C) fell below the thresholds for classical intercalators, whereas CD spectroscopy detected no B-to-Z transition but suggested localized helix compaction (B-to-φ transition) through minor band intensity changes. Hydrodynamic measurements further excluded intercalation, as DNA viscosity remained largely invariant ($\Delta\eta < 5\%$) despite IMDP addition, with initial viscosity reduction attributed to groove binding-induced helix curvature. Critically, the ionic strength independence ($\Delta F < 3\%$ under 150 mM NaCl) ruled out electrostatic interactions. Molecular docking simulations revealed the structural basis of this interaction.

Integrated multispectral approaches—including UV-vis absorption spectroscopy, fluorescence quenching, and circular dichroism (CD) spectroscopy—combined with thermal stability analysis collectively demonstrated that IMDP binding does not significantly perturb the conformational stability of the DNA double helix. This result suggests that the possible reason for IMDP's action is the spatial hindrance created after its binding with DNA.

The steric hindrance imposed by IMDP binding likely increases localized spatial constraints within the DNA helix, thereby obstructing the activity of DNA-associated enzymes (*e.g.*, topoisomerases) or the binding of transcription factors. Such interference may mechanistically disrupt critical processes, including DNA replication and transcription.

This study confirms the binding capacity of IMDP to double-stranded DNA, although its sequence specificity remains undetermined. Notably, pharmacokinetic evidence suggests that IMDP preferentially accumulates in DNA-rich tissues (*e.g.*, liver and kidneys) *in vivo*—a phenomenon potentially attributable to its nonspecific DNA-binding properties.[54] Further investigations to delineate its binding specificity could enable structural modifications aimed at minimizing off-target toxicity while enhancing therapeutic efficacy.

Author contributions

Yuxin Yu and Wanxin Luo designed the study and drafted the manuscript. Yuxin Yu, Wanxin Luo, YiWen Zhong, and Yidan Bai performed the experiments. Yuxin Yu, Wanxin Luo, Donfang Li, and Sen Wang participated in the data analysis.

Conflicts of interest

The authors confirm that there is no conflict of interest in the content of this article.

Data availability

Data will be made available on request.

Acknowledgements

This research was supported by grants from the National Key Research and Development Program of China (grant no. 2022YFD1801700), the National Natural Science Foundation of China (grant no. 32172879), and Top-notch Young Talent Supporting Program to Lan He (grant no.), and the Fundamental Research Funds for the Central Universities (grant no. 2262022DKYJ001 and 2662020DKPY016).

References

1 R. Bera, B. K. Sahoo, K. S. Ghosh and S. Dasgupta, *Int. J. Biol. Macromol.*, 2008, **42**, 14–21.
2 Y. Ni, M. Wei and S. Kokot, *Int. J. Biol. Macromol.*, 2011, **49**, 622–628.
3 Q. Hu, H. Li, L. Wang, H. Gu and C. Fan, *Chem. Rev.*, 2019, **119**, 6459–6506.
4 X. Huang, N. T. Blum, J. Lin, J. Shi, C. Zhang and P. Huang, *Mater. Horiz.*, 2021, **8**(1), 78–101.
5 A. Haque, K. M. Alenezi, M. S. Khan, W.-Y. Wong and P. R. Raithby, *Chem. Soc. Rev.*, 2023, **52**, 454–472.
6 W. J. Pichler, *Allergy*, 2022, **77**, 404–415.
7 S. U. Rehman, T. Sarwar, M. A. Husain, H. M. Ishqi and M. Tabish, *Arch. Biochem. Biophys.*, 2015, **576**, 49–60.
8 H. M. Berman, J. Westbrook, Z. Feng, G. Gilliland, T. N. Bhat, H. Weissig, I. N. Shindyalov and P. E. Bourne, *Nucleic Acids Res.*, 2000, **28**, 235–242.
9 M. Akhoundi, T. Downing, J. Votýpka, K. Kuhls, J. Lukeš, A. Cannet, C. Ravel, P. Marty, P. Delaunay, M. Kasbari, B. Granouillac, L. Gradoni and D. Sereno, *Mol. Aspects Med.*, 2017, **57**, 1–29.
10 P. Kour, P. Saha, D. K. Sharma and K. Singh, *Int. J. Biol. Macromol.*, 2024, **256**, 128401.
11 B. I. Schweitzer, A. P. Dicker and J. R. Bertino, *FASEB J.*, 1990, **4**, 2441–2452.
12 D. G. Lambie and R. H. Johnson, *Drugs*, 1985, **30**, 145–155.
13 B. R. E. Ansell, M. J. McConville, S. Y. Ma'ayeh, M. J. Dagley, R. B. Gasser, S. G. Svärd and A. R. Jex, *Biotechnol. Adv.*, 2015, **33**, 888–901.
14 C. C. Koh, K. J. Gollob and W. O. Dutra, *Cell Death Dis.*, 2023, **14**, 450.
15 A. H. Lee, L. S. Symington and D. A. Fidock, *Microbiol. Mol. Biol. Rev.*, 2014, **78**, 469–486.
16 P. J. McLaughlin and L. P. Keegan, *Biochem. Soc. Trans.*, 2014, **42**, 1159–1167.
17 F. J. Mendoza, A. Pérez-Écija, L. S. Kappmeyer, C. E. Suarez and R. G. Bastos, *Front. Vet. Sci.*, 2024, **11**, 1459989.
18 M. Azhar, J. A. Gadahi, B. Bhutto, S. Tunio, W. A. Vistro, H. Tunio, S. Bhutto and T. Ram, *Heliyon*, 2023, **9**, e17172.
19 H. J. Vial and A. Gorenflot, *Vet. Parasitol.*, 2006, **138**, 147–160.
20 S. Gupta, K. Sethi, S. Vohra, S. Gupta, R. Rani, S. Kumar and R. Kumar, *Vet. Parasitol.*, 2025, **338**, 110558.
21 M. A. Husain, Z. Yaseen, S. U. Rehman, T. Sarwar and M. Tabish, *FEBS J.*, 2013, **280**, 6569–6580.
22 T. Gustavsson and D. Markovitsi, *Acc. Chem. Res.*, 2021, **54**, 1226–1235.
23 T. Sarwar, S. U. Rehman, M. A. Husain, H. M. Ishqi and M. Tabish, *Int. J. Biol. Macromol.*, 2015, **73**, 9–16.
24 G. Wang and K. M. Vasquez, *Nat. Rev. Genet.*, 2023, **24**, 211–234.
25 M. Kumar, M. Ansari and A. Ansari, *Spectrochim. Acta, Part A*, 2023, **284**, 121774.
26 M. H. Garner and C. Corminboeuf, *Chem. Commun.*, 2021, **57**, 6408–6411.
27 K. Thimmaiah, A. G. Ugarkar, E. F. Martis, M. S. Shaikh, E. C. Coutinho and M. C. Yergeri, *Nucleosides, Nucleotides Nucleic Acids*, 2015, **34**(5), 309–331.
28 N. J. Upoma, N. Akter, F. K. Ferdousi, M. Z. Sultan, S. A.-O. Rahman, A. A.-O. Alodhayb, K. A. Alibrahim and A. A.-O. Habib, *ACS Omega*, 2024, **9**(20), 22325–22335.
29 M. Ganeshpandian, R. Loganathan, E. Suresh, A. Riyasdeen, M. A. Akbarsha and M. Palaniandavar, *Dalton Trans.*, 2014, **43**, 1203–1219.
30 N. A. Rejali, F. D. Ye, A. M. Zuiter, C. C. Keller and C. T. Wittwer, *Nucleic Acids Res.*, 2021, **49**, 4574–4585.
31 F. Zsila, *Phys. Chem. Chem. Phys.*, 2015, **17**, 24560–24565.
32 A. Basu and G. Suresh Kumar, *J. Agric. Food Chem.*, 2014, **62**, 317–326.
33 A. Basu and G. Suresh Kumar, *J. Biomol. Struct. Dyn.*, 2015, **34**, 935–942.
34 J. Li, H. Liu, R. Zuo, J. Yang and N. Li, *Chemosphere*, 2020, **249**, 126034.
35 X.-X. Zhang, S. L. Brantley, S. A. Corcelli and A. Tokmakoff, *Commun. Biol.*, 2020, **3**, 525.
36 A. Dearing, P. Weiner and P. A. Kollman, *Nucleic Acids Res.*, 1981, **9**, 1483–1497.
37 H. Liu, Y. Dong, J. Wu, C. Chen, D. Liu, Q. Zhang and S. Du, *Sci. Total Environ.*, 2016, **566–567**, 1–7.
38 Z. Malek-Esfandiari, A. Rezvani-Noghani, T. Sohrabi, P. Mokaberi, Z. Amiri-Tehranizadeh and J. Chamani, *J. Fluoresc.*, 2023, **33**, 1537–1557.
39 A. H. Hegde, S. N. Prashanth and J. Seetharamappa, *J. Pharm. Biomed. Anal.*, 2012, **63**, 40–46.
40 T. Sarwar, H. M. Ishqi, S. U. Rehman, M. A. Husain, Y. Rahman and M. Tabish, *Int. J. Biol. Macromol.*, 2017, **98**, 319–328.
41 B. Kalyani Bhardwaj, A. James, J. Tomy, K. B. Shalini and P. S. Suresh, *J. Biomol. Struct. Dyn.*, 2025, **43**(16), 9224–9235.
42 M. F. Dehkordi, S. Farhadian, F. Hashemi-Shahraki, B. Rahmani, S. Darzi and G. Dehghan, *Int. J. Biol. Macromol.*, 2023, **235**, 123713.
43 J. Kypr, I. Kejnovská, D. Renciuk and M. Vorlícková, *Nucleic Acids Res.*, 2009, **37**, 1713–1725.
44 N. Holmgaard List, J. Knoops, J. Rubio-Magnieto, J. Idé, D. Beljonne, P. Norman, M. Surin and M. Linares, *J. Am. Chem. Soc.*, 2017, **139**, 14947–14953.
45 Y.-M. Chang, C. K. M. Chen and M.-H. Hou, *Int. J. Mol. Sci.*, 2012, **13**, 3394–3413.
46 S. K. Shukla and J.-P. Mikkola, *Front. Chem.*, 2020, **8**, 598662.
47 H. Tateishi-Karimata and N. Sugimoto, *Nucleic Acids Res.*, 2014, **42**, 8831–8844.
48 A. Kellett, Z. Molphy, C. Slator, V. McKee and N. P. Farrell, *Chem. Soc. Rev.*, 2019, **48**, 971–988.

49 S. Forli, R. Huey, M. E. Pique, M. F. Sanner, D. S. Goodsell and A. J. Olson, *Nat. Protoc.*, 2016, **11**, 905–919.
50 J. B. Chaires, *Arch. Biochem. Biophys.*, 2006, **453**, 26–31.
51 H. Liu, X. Huang, J. Shen, X. Luo, M. Li, B. Xiong, G. Chen, J. Shen, Y. Yang, H. Jiang and K. Chen, *J. Med. Chem.*, 2002, **45**, 4816–4827.
52 B. Tuvshintulga, T. Sivakumar, N. Yokoyama and I. Igarashi, *Int. J. Parasitol.: Drugs Drug Resist.*, 2019, **9**, 87–92.
53 B. Tuvshintulga, T. Sivakumar, A. B. Nugraha, B. Ahedor, E. Batmagnai, D. Otgonsuren, M. Liu, X. Xuan, I. Igarashi and N. Yokoyama, *J. Infect. Dis.*, 2022, **225**, 238–242.
54 G. E.-S. Batiha, A. M. Beshbishy, L. M. Alkazmi, E. H. Nadwa, E. K. Rashwan, N. Yokoyama and I. Igarashi, *PLoS Neglected Trop. Dis.*, 2020, **14**, e0008489.